Limnol. Oceanogr., 35(7), 1990, 1486–1502

Modeling spectral diffuse attenuation, absorption, and scattering coefficients in a turbid estuary

Charles L. Gallegos and David L. Correll
Smithsonian Environmental Research Center, P.O. Box 28, Edgewater, Maryland 21037

J. W. Pierce
Museum of Natural History, Smithsonian Institution, Washington, D.C. 20560

Abstract

Spectral diffuse attenuation coefficients were measured in the Rhode River and Chesapeake Bay, Maryland, on 28 occasions in 1988 and 1989. The model of Kirk was used to extract scattering and absorption coefficients from the measurements in waters considerably more turbid than those in which the model was previously applied. Estimated scattering coefficients were linearly related to mineral suspended solids. Estimates of total absorption coefficients were decomposed as the sum of contributions by water, dissolved organic matter, phytoplankton chlorophyll, and particulate detritus, each having a characteristic spectral shape. The 1988 data were used to develop a model of scattering and absorption coefficients based on the specific curves regressed against water-quality parameters. Diffuse attenuation coefficients in the 1989 data ranging from 1 to 10 m^{-1} and photic depths ranging from <1 to 4.5 m were predicted with a C.V. of about 25%.

The problem of estimating concentrations of water-quality constituents from optical measurements was indeterminate due to the similarity in shape of the specific curves of dissolved substances and depigmented particulates. Chlorophyll concentration could be estimated because it was strongly related to water-corrected absorption in the 670-nm waveband, but several outliers occurred due to biological variability in specific absorption of pigments.

The penetration and availability of light underwater is of fundamental interest in aquatic systems. The interactions of light availability, its spectral energy distribution, and the physiology of phytoplankton set fundamental constraints on the rate of primary production of a water column (Platt et al. 1984). The simulation of photon flux density (PFD) as a function of depth and particulate and dissolved substances usually represents a point of departure in models of planktonic processes. Prediction of the availability and propagation of light underwater from a knowledge of its suspended and dissolved load may be referred to as the direct problem. The inverse problem, that of inferring the concentrations of dissolved and particulate constituents in the water from measured optical properties (e.g. spectral reflectance or beam attenuation) is also of great interest currently. It is generally agreed that estimates of phytoplankton chlorophyll content from satellite imagery will be essential for improving estimates of global oceanic primary production (Platt and Sathyendranath 1988).

In estuarine waters there are important roles for both the direct and inverse problems. Growth of submerged aquatic vegetation (SAV) depends on the quantity and quality of light available at the bottom of a shallow water column; solution of the direct problem for such waters would facilitate prediction of the light available for SAV from measurements of water quality. Similarly, monitoring the efficacy of pollution abatement efforts over large areas with remote sensing requires solution of the inverse problem for the areas of interest. Estuaries offer several advantages for conducting optical studies. Easy access from shore laboratories in small boats permits frequent coverage at modest expense. Work can often be done in relatively sheltered areas, making it possible to take measurements near the surface. Because of the strong spatial gradients in most estuaries, several water types can be sampled in a short period.

Acknowledgments

We thank J. Duls, S. Hedrick, J. Calem, and C. Hayne for assistance with field sampling and laboratory analyses, and A. Weidemann, T. Bannister, and an anonymous referee for comments on the manuscript.

This study was supported by the Smithsonian Institution Environmental Sciences Program.

In spite of the potential importance of understanding the optical properties of estuaries, most optical studies have focused on deep, clear oceanic regions (e.g. Morel 1988; Spinrad 1989). At least two factors have motivated this emphasis. Simple areal considerations suggest that oceanic regions are most important for estimating global phytoplankton production. Second, a theoretical framework to predict scattering, Mie theory, is available for testing against observations in oceanic regions. Multiple scattering in turbid estuarine waters greatly complicates the mathematical analysis of radiative transfer (van de Hulst 1957; Timofeeva 1974). In estuaries and turbid waters generally, the lack of a theoretical framework has led to reliance on empirical regressions between measured optical properties and water-quality parameters (e.g. Pierce et al. 1986) or Monte Carlo simulations of the underwater light field (Kirk 1981, 1984).

In optical studies it is necessary to distinguish between inherent optical properties, which are determined solely by the contents of the water, and apparent optical properties, which are a function of both the content of the water and the ambient light field; i.e. other things being equal, apparent optical properties will vary with, for example, solar zenith angle, cloud cover, or atmospheric aerosol content (Preisendorfer 1976). This distinction suggests that solution of either the direct or inverse problem will be facilitated by extraction of inherent optical properties from field measurements of light penetration with depth.

Inherent optical properties have the added advantage that the contributions of individual components to the overall property are strictly additive (Jerlov 1976). For example, the total absorption coefficient at a wavelength λ, $a_t(\lambda)$, is an inherent optical property and can be decomposed as the sum of the absorption due to pure water $a_w(\lambda)$, dissolved organic matter $a_d(\lambda)$, and particulate material $a_p(\lambda)$ (Prieur and Sathyendranath 1981). (Units given in list of symbols.) That is

$$a_t(\lambda) = a_w(\lambda) + a_d(\lambda) + a_p(\lambda).$$

Absorption by particulate material may be further divided into the contribution due to phytoplankton, $a_{ph}(\lambda)$ and that due to mineral and organic detritus, $a_x(\lambda)$.

Here we apply the model of Kirk (1984) to measurements of spectral diffuse attenuation coefficients in the Rhode River and nearby Chesapeake Bay, Maryland—waters considerably more turbid (photic depths <1–4 m) than those in which Kirk's (1984) model was previously applied (Phillips and Kirk 1984; Weidemann and Bannister 1986). We use it to extract estimates of absorption and scattering coefficients—two in-

Significant symbols

λ	Wavelength, nm
$a_t(\lambda)$	Total spectral absorption coefficient, m^{-1}
$a_d(\lambda)$, $a_p(\lambda)$, $a_{ph}(\lambda)$	Spectral absorption coefficients of dissolved substances, particulate matter, and phytoplankton, m^{-1}
$a^*_{ph}(\lambda)$	Spectral absorption coefficient of phytoplankton normalized to [Chl *a*], m^2 (mg Chl *a*)$^{-1}$
$a_x(\lambda)$, $a_w(\lambda)$	Spectral absorption coefficients of nonpigmented particles and water, m^{-1}
b	Scattering coefficient, m^{-1}
$k_d(\lambda)$	Spectral diffuse attenuation coefficient for downwelling irradiance, m^{-1}
μ_0	Cosine of the solar zenith angle after refraction at the air–water interface
$G(\mu_0)$, g_1, g_2	Empirical function and parameters that determine the influence of scattering on diffuse attenuation coefficient $G(\mu_0) = g_1\mu_0 + g_2$
β	Path-length amplification factor for particulate absorption measured on glass-fiber filters
$I_0(\lambda)$, $I_z(\lambda)$	Spectral, downwelling photon flux density (400–700 nm) incident at the surface (0) and penetrating to depth *z*, μmol quanta m^{-2} s^{-1} nm^{-1}
PAR	Photosynthetically available radiation, μmol quanta m^{-2} s^{-1}, $= \int_{400}^{700} I_z(\lambda)\, d\lambda$
PUR	Photosynthetically usable radiation, i.e. the photon flux density weighted by the spectral absorption of phytoplankton $= \int_{400}^{700} I_z(\lambda) a^*_{ph}(\lambda)\, d\lambda$
z	Depth, m
z_p(PAR), z_p(PUR)	Depth of penetration of 1% of surface incident irradiance for PAR and PUR, m
[DOC], [TOC]	Dissolved and total organic C concn, mg $liter^{-1}$
[MSS], [TSS]	Mineral and total suspended solids concn, mg $liter^{-1}$
[Chl *a*]	Chl *a* concn, μg $liter^{-1}$

herent optical properties. We then relate the inherent optical coefficients to measured water-quality parameters based on specific absorption curves of dissolved organic matter (DOM), phytoplankton chlorophyll (Chl), and particulate detritus.

Materials and methods

Study site—Measurements of spectral diffuse attenuation coefficients and water-quality parameters were made in the Rhode River and at one station (73) on the mainstem of Chesapeake Bay near the mouth of the Rhode River (Fig. 1). The Rhode River is a turbid, eutrophic subestuary on the western shore of Chesapeake Bay. Mean depth of the river is 2 m, and maximal depth is nearly 5 m; depth at station 73 on Chesapeake Bay is 8 m. Salinity varies seasonally from ~5 to 20‰ at the mouth of the river and from 0 to 17‰ at the head. Fifteen profiles measured between 20 July and 27 October 1988 were used for model development. Twelve profiles measured in 1989 were used for model evaluation.

Instrumentation—The underwater spectral radiometer we used is a modification of the design described by Goldberg et al. (1985). The instrument housing is made of stainless steel (40 × 40 × 20 cm, $l \times w \times h$). The top plate has cutouts for 14 cosine-correcting Teflon diffusers. Light passing through the diffusers is collimated and passed through an interference filter (Corion Corp.) onto a silicon detector. One detector measures broadband visible energy after passing through a total infrared suppressor (Corion Corp.) instead of an interference filter. A similar diffuser-infrared suppressor-detector assembly measures visible irradiance above the surface to correct for the effects of cloud cover or changes in solar zenith angle during the profile. The interference filters isolate regions of the visible and near-infrared spectrum that vary in bandwidth (Fig. 2). Narrowest bandwidths (10 nm) are used in the regions of the spectrum most affected by absorption by phytoplankton pigments; 25- and 40-nm bandwidths are used elsewhere. Diffuse attenuation coefficients are reported and plotted at the nominal wavelengths of maximal transmittance (Table 1). One filter, centered at 500 nm, was inadvertantly duplicated and the 550-nm filter omitted, leaving a gap in the middle of the spectrum (Fig. 2).

Current output from the silicon detectors was converted to voltage and recorded on a Campbell 21X data logger. Sensor output was read every 0.5 s and averaged for 1 min at each depth. Although not required for calculation of diffuse attenuation coefficients, sensors were calibrated in air with a standard lamp (Eppley Laboratories, EV 22) traceable to the National Bureau of Standards. Immersion coefficients (e.g. Kirk 1983) were not determined. At the start of a profile, reference values in air were calculated for each sensor by normalizing to the voltage of the deck cell. Readings at each depth were similarly normalized to the deck cell, and the percentage of the reference value for each waveband was calculated. Diffuse attenuation coefficients for downwelling spectral irradiance, k_d, were then calculated from the slope of a regression of log-transformed percentages against depth. Thus, by normalizing, the calibration factors cancel, and, by log transforming, the undetermined immersion coefficients affect only the calculated intercepts of the regressions, which were not considered in this analysis.

Weather conditions during the profiles varied from clear to variably cloudy. Preliminary analysis of data from cloudy periods indicated that coefficients of determination for computed k_d could be raised from <0.8 to >0.94 by the procedure of normalizing to the deck reading. The instrument was suspended from a boom 3 m long (1–5 attenuation lengths in these waters) on the sunward side of the boat.

Profiles of quantum scalar irradiance (400–700 nm) were measured with a Biospherical Instruments QSP-170 4π collector and QSR-250 integrator. Diffuse attenuation coefficients for quantum scalar irradiance, k_q(PAR), were calculated from regression of log-transformed readings against depth. Secchi depth was measured with a 20-cm solid white disk.

Water-quality parameters—At each station water was sampled with a 2-liter polyethylene bottle with a lid outfitted with two

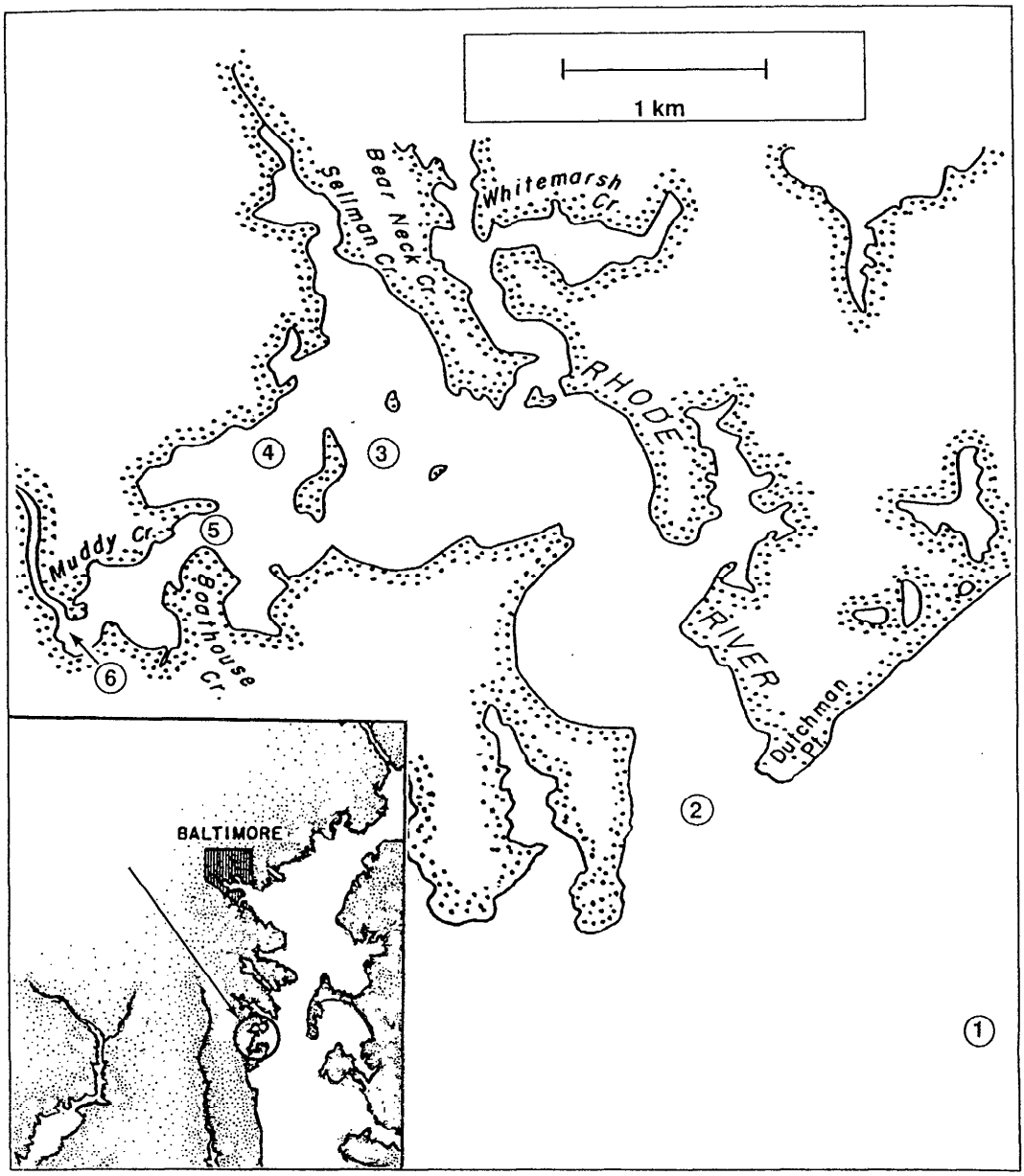

Fig. 1. Map of Rhode River showing station locations. Inset shows location of Rhode River on Chesapeake Bay.

holes, one with a fitting 5-cm long for escape of air, and the other for intake of water. Discrete samples were collected from 10 cm below the surface and from 10 cm above the bottom; an integrated sample was collected by lowering and raising the bottle at a constant rate in less time than required to completely fill the bottle. In many instances, no light was detectable near the bottom, and energy was rarely detectable below 1.5 m in the 410-nm waveband. Therefore only measurements from the near-surface samples are used for correlation with optical properties.

Aliquots were filtered immediately

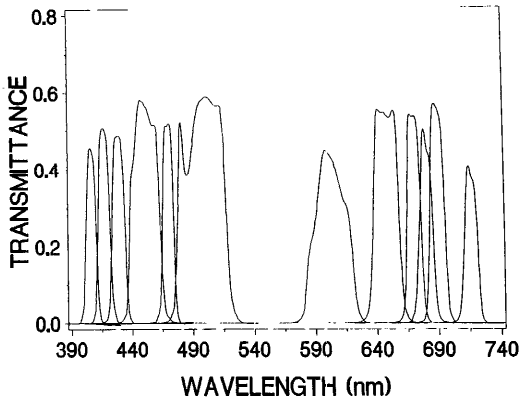

Fig. 2. Transmittance spectra (dimensionless) of interference filters used in the underwater spectral radiometer.

through 0.2-μm Nuclepore polycarbonate filters and returned to the laboratory on ice. Total and dissolved organic C (TOC and DOC respectively) were determined by potassium dichromate-sulfuric acid oxidation of whole and filtered samples with back-titration of the residual dichromate solution. Samples for TOC and DOC were frozen up to 8 months before analysis. Total suspended solids (TSS) and mineral suspended solids (MSS) were determined by filtering onto tared 0.4-μm Nuclepore filters, gravimetrically determining weight gain of the filter, firing to destroy organic matter and filter, and reweighing the residue. Whole-water samples were filtered through Whatman GF/F filters for spectrophotometric determination of Chl *a*, *b*, *c*, and carotenoids. Filters were extracted in 10 ml of 90% acetone overnight at 4°C either immediately or after freezing for <2 weeks. Absorbances of extracts were determined at selected wavelengths and pigment concentrations determined by the equations of Jeffrey and Humphrey (1975).

Table 1. Wavelength (nm) of maximal transmission, bandwidths, and maximal transmission (%) of interference filters used in the underwater spectral radiometer.

Nominal wavelength	Half-power wavelengths		Central wavelength	Transmittance max
	Lower	Upper		
410	401	410	406	46
420	412	422	416	50
430	424	435	430	49
450	438	463	448	58
500	478	517	502	58
600	588	619	598	47
650	637	658	641	55
670	664	676	669	54
680	675	686	679	50
690	683	696	688	57
720	711	722	715	40

Optical measurements in the laboratory—Absorption due to dissolved substances was determined on filtered samples (0.2-μm Nuclepore) in a Cary spectrophotometer with a 10-cm cell against a distilled water reference. Measured transmittance was converted (base *e*) to an absorption coefficient (m^{-1}).

Absorption by particulate matter was determined with an Aminco DW-2 spectrophotometer; on one date in 1988 and on all dates in 1989, absorption by particulate matter was measured with an EG&G gamma spectrometer interfaced to a LiCor 1800-12 integrating sphere. For measurement in the DW-2 spectrophotometer, water was filtered onto a 47-mm Whatman GF/F filter with a 25-mm filter holder and tower placed near the edge of the filter. The filter was trimmed to fit in the slot usually occupied by the quartz diffuser immediately in front of the end-on photomultiplier tube. In this configuration, the reference beam passed through the clean side of the filter and the sample beam through the particulate material. The filter was saturated with distilled water just before placement in the holder and scanned at a rate of 2 nm s^{-1} from 400 to 750 nm. Volume filtered was adjusted to be readable at full scale of 0.5 AU. Absorbances were recorded by a plotter and digitized at 2-nm increments. Digitized absorbances were multiplied by 2.303 to convert to base *e* and multiplied by A/V, where A was area of the filter (m^2) and V the volume filtered (m^3), to convert to units of m^{-1}.

The procedure used with the integrating sphere was very similar, except that the filter was not trimmed, and the reference used was the average of five scans of clean, water-saturated GF/F filters. Filters were scanned at 2-nm increments from 400 to 750 nm, and raw detector voltages were stored in computer files. Absorbance was calculated from raw detector voltages in direct analogy to spectrophotometric procedures,

$$T(\lambda) = E_s(\lambda)/E_r(\lambda)$$

$$a_p(\lambda) = \log[1/T(\lambda)]$$

where $E_s(\lambda)$ and $E_r(\lambda)$ are the detector voltages of light passing through the sample and reference filters and $T(\lambda)$ is transmittance. Residual absorbance at 750 nm was subtracted from measurements at all wavelengths (Kishino et al. 1985).

With both measurement systems, filters were depigmented by extraction in methanol for 1–4 h, followed by a second extraction for 15–30 min, rehydrated, and scanned again to determine absorption by mineral and organic detritus (Kishino et al. 1985, 1986).

Particulate absorbance measured on filters overestimates absorption relative to in situ conditions due to the increased path length traveled by the light passing through the particulate material and the filter (Kiefer and SooHoo 1982). To describe absorption in situ, we must divide the measured absorbances by a path-length amplification factor, β. We estimated β by noting that

$$a_t(\lambda) = a_w(\lambda) + a_d(\lambda) + a_p'(\lambda)/\beta \quad (1a)$$

or

$$\beta = a_p'(\lambda)/[a_t(\lambda) - a_w(\lambda) - a_d(\lambda)] \quad (1b)$$

where $a_p'(\lambda)$ is the measured absorbance of particulate material, $a_t(\lambda)$ was estimated from field data (*see below*), $a_w(\lambda)$ is known from published data (Smith and Baker 1981), and $a_d(\lambda)$ was determined as described above.

Estimates of β determined in this way varied from 2.63 to 4.06, with a mean of 3.31 (C.V. = 15%, n = 13). The value estimated for each profile was used in model development (i.e. determination of specific absorption curves for Chl and detritus) and the mean used for model evaluation. Our estimated range for β is similar to that determined by Kishino et al. (1985), 2.5–4.7, and somewhat higher than that determined by Mitchell and Kiefer (1984), ~1.5–2.5.

Estimation of optical coefficients from field data—Using a Monte Carlo model of the propagation of photons underwater, Kirk (1984) determined the following relationship between diffuse attenuation coefficient, k_d, and the total absorption and scattering coefficients, a_t and b:

$$k_d = \frac{1}{\mu_0}[a_t^2 + G(\mu_0)a_t b]^{1/2} \quad (2a)$$

and

$$G(\mu_0) = g_1\mu_0 - g_2 \quad (2b)$$

where μ_0 is the cosine of the solar zenith angle refracted at the air–water interface, which can be calculated from location and time of day. $G(\mu_0)$ is a coefficient that determines the relative contribution of scattering to vertical attenuation and is a function of optical depth. In this work we calculated k_d averaged from the surface down to the 1% light level, i.e. k_d(avg), and therefore used the values (Kirk 1984) $g_1 = 0.425$ and $g_2 = 0.190$.

If a_t and b are unknown, Eq. 2a is undetermined if measurements of k_d(avg) alone are available. Phillips and Kirk (1984) used simultaneous measurements of spectral beam transmittance, $c(\lambda)$, and the relation

$$c(\lambda) = a_t(\lambda) + b(\lambda) \quad (3)$$

to close the equations. They found that estimated scattering coefficients were nearly invariant with wavelength—a result to be expected whenever, as in the waters we examined, scattering is predominantly by particles larger than the wavelength of light (Jerlov 1976). We calculated b by assuming that water itself is the only significant absorbing substance in the 720-nm waveband with $a_w(720) = 1.002$ m^{-1}. The value we used for $a_w(720)$ differs from the reported value of 1.169 m^{-1} at 720 nm; the value used is the average of interpolated values of $a_w(\lambda)$ over the half-power bandwidth of the 720-nm filter, which is actually centered at 715 nm (Table 1). We then calculated an estimated scattering coefficient, $b(720)$, by rearranging Eq. 2 and used that value for all wavebands.

Results

Diffuse attenuation, scattering, and absorption coefficients—The minimal k_d always occurred in the 600-nm waveband and ranged from 0.79 to 3.13 m^{-1} (Fig. 3). Maximum k_d occurred in the 410- or 420-nm wavebands. The clearest water was encoun-

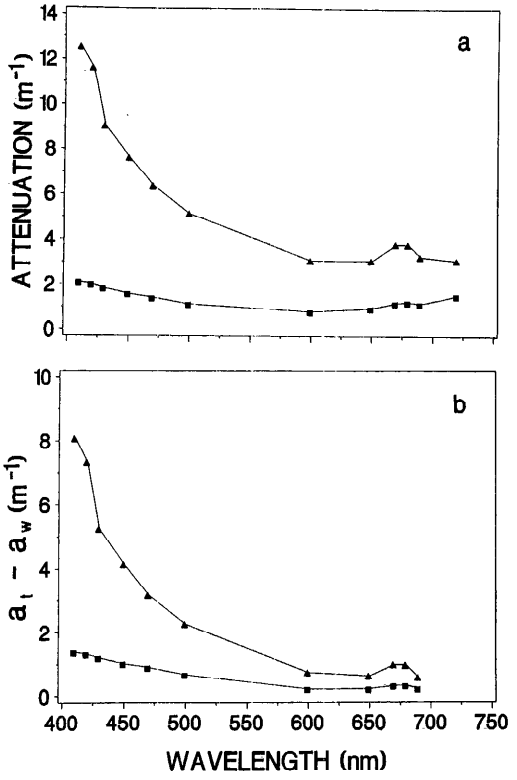

Fig. 3. Spectra of optical coefficients for stations having the shallowest (▲) and deepest (■) photic depths encountered in 1988. a. Diffuse attenuation coefficient. b. Total absorption coefficient corrected for absorption by water.

tered at the mouth of the Rhode River on 27 October 1988 [$k_d(410) = 2.10$ m^{-1}]. The most turbid water was encountered at station 5, a shallow location with high concentrations of MSS. Maximal k_d was 12.4 m^{-1} in the 410-nm waveband.

Estimated scattering coefficients ranged from 1.73 to 55.3 m^{-1}, and the ratio of the scattering coefficient to the minimal total absorption coefficient, b/a_t(min), ranged from 2.1 to 78.9 (Table 2). For four of the profiles b/a_t(min) exceeded 20, the highest value used by Kirk (1984) in deriving Eq. 2, but the effect of extrapolating this relationship on estimates of optical coefficients cannot be determined. Estimates of b were highly correlated with [MSS] (Fig. 4a, Table 3). Least-squares regression gave

$$b = 2.41[\text{MSS}] + 0.32. \quad (4)$$

Estimated scattering coefficients were used with Eq. 2 to estimate $a_t(\lambda)$ at other wavebands for each profile. Typically, minima were in the 600-nm waveband, and $a_t(\lambda)$ frequently exhibited local peaks in the 670- and 680-nm wavebands in the presence of high [Chl]; subtraction of $a_w(\lambda)$ generally shifted the minimum to 690 nm (Fig. 3b).

Specific absorption of dissolved matter—Spectrophotometric scans of filtered estuary water showed the negative exponential decrease through the visible region of the spectrum typical of other studies (Bricaud et al.

Table 2. Dates, stations, and ancillary data for profiles of spectral diffuse attenuation. [DOC], [TSS], [MSS]—mg liter^{-1}; [Chl *a*]—μg liter^{-1}; SD—Secchi depth, m; k(QSR)—diffuse attenuation of quantum scalar irradiance, m^{-1}; b—m^{-1}; a_t(min)—minimum total absorption coefficient. Dates are those used for model development (*see text*). Undefined terms explained in list of symbols.

1988	Sta.	[DOC]	[TSS]	[MSS]	[Chl *a*]	SD	k(QSR)	b	b/a_t(min)
20 Jul	2	—	13.0	4.6	—	0.80	2.05	12.5	2.1
20 Jul	4	—	13.8	5.6	—	0.50	2.48	22.5	17.2
2 Aug	4	6.1	9.7	4.7	10.0	0.75	—	15.6	19.9
2 Aug	6	6.9	21.9	14.3	63.6	0.45	—	34.3	34.6
1 Sep	1*	6.5	24.5	4.2	173.2	0.70	2.99	14.2	14.1
1 Sep	4	6.3	12.9	8.0	49.4	0.35	2.46	21.4	24.8
22 Sep	1	2.9	5.1	3.8	30.7	2.25	—	7.9	12.3
22 Sep	4	5.0	11.6	5.7	65.7	0.75	—	19.2	20.9
22 Sep	73	2.8	2.3	1.5	16.8	0.50	—	2.0	3.5
12 Oct	3	3.5	6.2	4.0	21.5	0.80	1.40	9.5	17.3
12 Oct	4	3.5	7.3	5.5	18.4	0.55	1.71	10.3	17.6
12 Oct	5	3.6	29.6	23.3	28.3	0.20	2.73	55.3	78.9
27 Oct	2	2.6	4.7	2.6	19.8	1.50	1.10	1.7	3.6
27 Oct	3	2.7	4.0	2.4	5.9	1.30	1.27	2.8	5.9
27 Oct	4	3.2	9.1	6.3	17.7	0.55	1.79	9.1	16.6

* k_d estimated for only 720- and 600-nm bandwidths because the depth increment was too coarse.

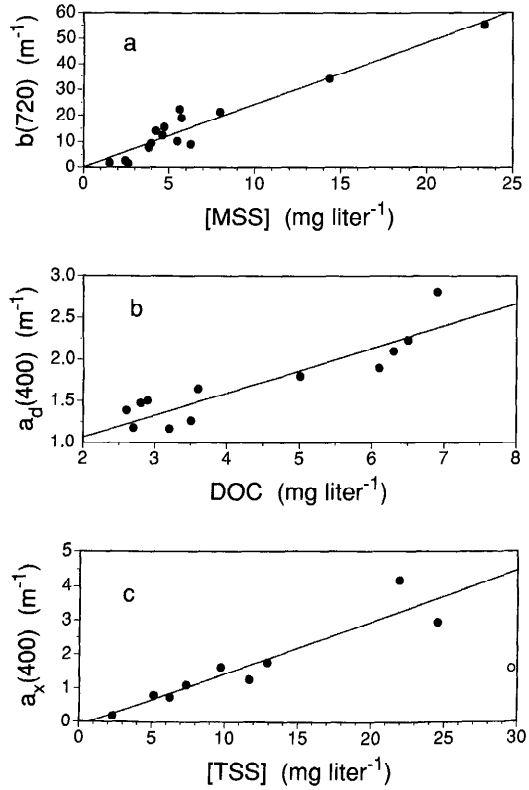

Fig. 4. Regressions of optical coefficients against water quality parameters. a. Scattering coefficient estimated from diffuse attenuation coefficient at 720 nm against [MSS]. b. Absorption by dissolved matter at 400 nm against DOC. c. Absorption of depigmented particulate material at 400 nm against [TSS]; one outlier (O) was omitted from regression.

1981). The average spectral slope over 400–550 nm was 0.012 nm^{-1}. Absorption by dissolved matter at 400 nm was correlated with DOC (Fig. 4b, Table 3), suggesting that absorption due to dissolved substances in this system can be estimated by

$$a_d(\lambda) = [0.27\ \mathrm{DOC} + 0.53]\ \exp[-0.012\ (\lambda - 400)]. \quad (5)$$

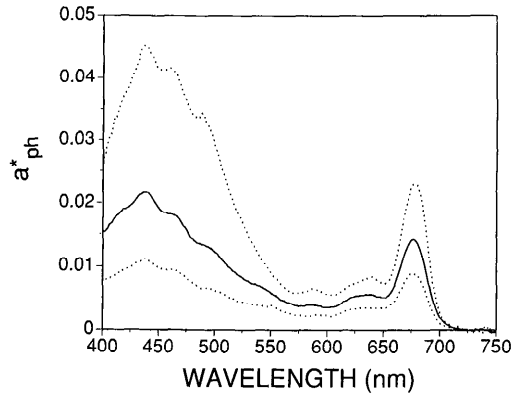

Fig. 5. Range (·····) and mean (——) specific absorption by phytoplankton Chl in m^2 (mg Chl a)$^{-1}$.

Absorption by particulate matter—After estimation of β by Eq. 1b, measured particulate absorbance, corrected for pathlength amplification, was partitioned into contributions due to mineral and organic detritus, a_x, and due to phytoplankton and their extractable degradation products, a_{ph}. Detrital absorption showed a typical negative exponential decline (Kishino et al. 1985), with a mean spectral slope of 0.0104 nm^{-1} (C.V. = 15.5%, n = 9). Detrital absorption at 400 nm was correlated with [TSS] (Fig. 4c, Table 3). Thus, we estimate a_x by

$$a_x(\lambda) = [0.153\ \mathrm{TSS} - 0.13]\ \exp[-0.0104\ (\lambda - 400)]. \quad (6)$$

Absorption due to phytoplankton was divided by [Chl] to calculate the Chl-specific absorption of phytoplankton, $a^*_{ph}(\lambda)$. Peak values of $a^*_{ph}(\lambda)$ occurred at 440 nm and ranged from 0.01 to 0.045 m^2 (mg Chl a)$^{-1}$ (Fig. 5, Table 4).

The direct model—Equations 5 and 6 and tabulated values of $a_w(\lambda)$ and $a^*_{ph}(\lambda)$ (Table 4) together with measurements of [DOC], [TSS], and [Chl a] give a complete set of

Table 3. Regression statistics for estimation of optical coefficients from water-quality parameters: SE—standard error; r^2—coefficient of determination; n—number of observations. a_d(400)—absorbance of dissolved matter at 400 nm; a_x(400)—absorbance of depigmented particles at 400 nm; other symbols as in Table 2. Units of dependent variables are m^{-1}; units of independent variables are mg liter^{-1}.

Dependent	Independent	Slope (SE)	Intercept (SE)	r^2	n
b	[MSS]	2.41(0.20)	0.33(4.21)	0.92	15
a_d(400)	[DOC]	0.27(0.04)	0.53(0.22)	0.81	13
a_x(400)	[TSS]	0.15(0.02)	−0.11(0.49)	0.87	9

Table 4. Average curve of specific absorption by phytoplankton Chl *a*; a^*_{ph} in m^2 (mg Chl *a*)$^{-1}$.

Wavelength	a^*_{ph}	Wavelength	a^*_{ph}
400	0.0203	550	0.0074
405	0.0218	555	0.0067
410	0.0239	560	0.0059
415	0.0250	565	0.0054
420	0.0261	570	0.0051
425	0.0270	575	0.0049
430	0.0286	580	0.0050
435	0.0298	585	0.0052
440	0.0298	590	0.0052
445	0.0284	595	0.0050
450	0.0268	600	0.0049
455	0.0265	605	0.0049
460	0.0268	610	0.0052
465	0.0262	615	0.0061
470	0.0249	620	0.0066
475	0.0233	625	0.0069
480	0.0217	630	0.0072
485	0.0207	635	0.0073
490	0.0207	640	0.0075
495	0.0197	645	0.0071
500	0.0182	650	0.0077
505	0.0166	655	0.0070
510	0.0151	660	0.0088
515	0.0138	665	0.0123
520	0.0125	670	0.0159
525	0.0112	675	0.0180
530	0.0103	680	0.0176
535	0.0097	685	0.0145
540	0.0088	690	0.0091
545	0.0083	695	0.0047
		700	0.0022

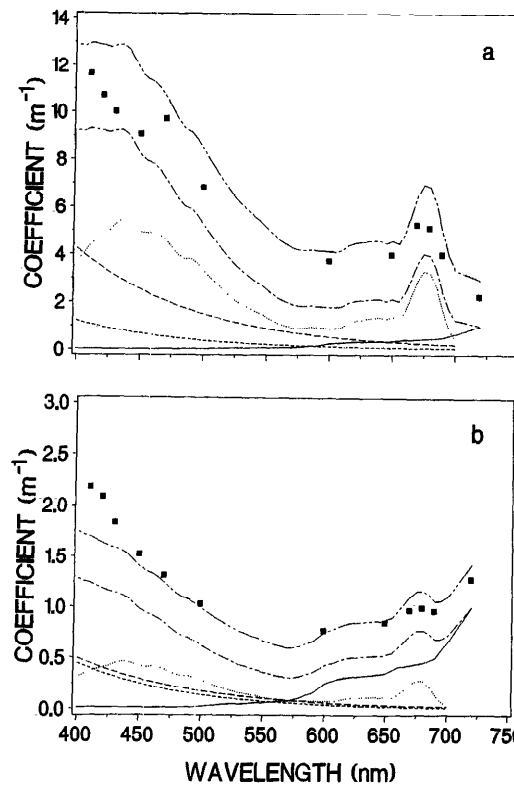

Fig. 6. Absorption and diffuse attenuation coefficients predicted by direct model (*see text*) and measured diffuse attenuation coefficients for stations having the shallowest (a) and deepest (b) photic depths encountered in 1989. Solid lines—$a_w(\lambda)$; short dashes—$a_d(\lambda)$; long dashes—$a_x(\lambda)$; dotted lines—$a_{ph}(\lambda)$; long and short dashes—$a_t(\lambda)$; long and doubled short dashes—predicted $k_d(\lambda)$; squares—measured $k_d(\lambda)$.

equations for estimating $a_t(\lambda)$ in the Rhode River and nearby Chesapeake Bay. Equation 4 with measurements of [MSS] predict b, thus closing Eq. 2 for estimating photic-zone-averaged $k_d(\lambda)$. Plots of predicted and observed spectra of $k_d(\lambda)$ for the stations with the shallowest and deepest photic depths encountered in the evaluation data set (Fig. 6) demonstrate that the overall magnitudes and spectral shapes are well predicted.

Data from 1989 provided a rigorous test of the model; [Chl] higher than any encountered in 1988 were found on two occasions, and three profiles exhibited substantial subsurface Chl maxima. For evaluation we plotted predicted vs. observed $k_d(\lambda)$ for $\lambda = 430$ and 670 (the wavebands of the radiometer closest to the Chl absorption peaks), for $\lambda = 600$ (typically the minimal k_d), and for $\lambda = 720$ (the best predictor of scattering, Fig. 7); we used [Chl] from the depth-integrated sample for profiles with subsurface Chl maxima and surface samples for all others. Over a range of observed k_d from 0.8 to 10 m^{-1}, predictions are unbiased, and the mean residual is 21% of the predicted value.

Vertical inhomogeneities in the concentrations of absorbing and scattering constituents pose special problems for detailed modeling of the underwater light field in turbid waters. At station 2 on 7 July 1989, a strong subsurface peak of Chl was observed at a depth of 0.5 m (Table 5). Estimates of $k_d(\lambda)$ based on the first three depth increments (0.1–0.25 m, 0.25–0.5 m, and 0.5–0.75 m) displayed strong depth dependence (Fig. 8a), with intensification of k_d in the 650–690-nm wavebands due to the in-

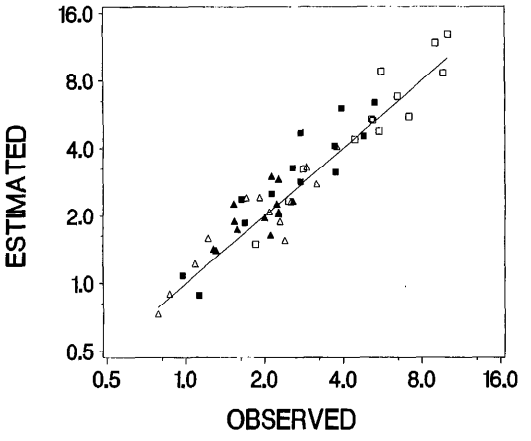

Fig. 7. Plot of estimated k_d on observed k_d (m^{-1}) from 1989 data set for 430-nm (□), 600-nm (△), 670-nm (■), and 720 nm (▲) wavebands.

creased [Chl] at 0.5 m. Measurements of particulate absorbance on samples from 0.1 m, 0.5 m, and the depth-integrated sample (Fig. 8b) also show the effect of the subsurface Chl peak.

In principle the depth-variation of $a_t(\lambda)$ could be modeled from laboratory measurements of $a_d(\lambda)$ and $a_p(\lambda)$ from different depth strata, but as yet it is not possible to convert these measurements to estimates of $k_d(\lambda)$, even if the depth variation of b were known. The modeling problem is that the values of g_1 and g_2 in Eq. 2b depend on optical depth and hence also on λ, due to the wavelength dependence of k_d. Furthermore, values g_1 and g_2 have been determined only for small depth increments about the 10% light level, and for the average k_d in a homogeneous water column from the surface down to the 1% light level. Thus, even though the magnitude and spectral shape of k_d(avg) is well predicted by the direct model with water-quality measurements from the depth-integrated samples (Fig. 8c), the interesting depth-dependent variability is lost. [Note that insufficient penetration of energy below 0.5 m in the 410-, 420-, and 430-nm wavebands prevented calculation of $k_d(\lambda)$ for those wave-

Table 5. Depth dependence of water-quality parameters at station 2 on 7 July 1989, a location having a pronounced subsurface Chl maximum. [DOC], [TSS], [MSS]—mg liter^{-1}; [Chl *a*]—μg liter^{-1}. Not determined—ND.

Depth (m)	[DOC]	[TSS]	[MSS]	[Chl]
0.1	6.9	3.7	2.3	55
0.5	ND	ND	ND	253
2.0	4.9	11.7	8.2	56
Integrated	6.0	7.6	4.5	114

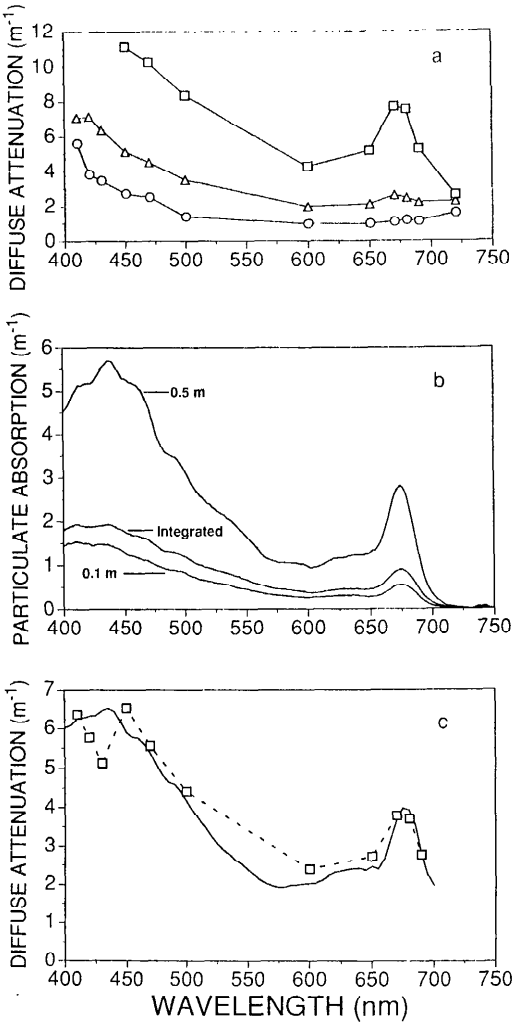

Fig. 8. Spectra of optical properties at different depths at station 2, 7 July 1989, a location having a pronounced subsurface Chl maximum. a. Diffuse attenuation coefficient calculated for three successive depth intervals near the surface: ○—0.10–0.25 m; △—0.25–0.5 m; □—0.5–0.75 m. b. Absorbance of particulate material measured on samples from 0.1 m, 0.5 m, and the depth-integrated sample. c. Diffuse attenuation coefficients calculated with measurements from 0.1 m down to the 1% light depth (- - - □ - - -) and values predicted by the direct model with water-quality measurements on the depth-integrated sample (——).

bands in the 0.5–0.75-m depth increment (Fig. 8a) and was responsible for the increase in k_d(avg) from the 430- to 450-nm wavebands (Fig. 8c).]

One of the principal applications of the direct model is prediction of light available for phytoplankton. We calculated the penetration of photosynthetically usable radiation (PUR, Morel 1981) for a standard solar spectrum (*Handbook of chemistry and physics* 1980) converted to quantum units for modeled and measured $k_d(\lambda)$. PUR is the photon flux density (PFD) that can be absorbed by the phytoplankton assemblage present; i.e. it is the PFD weighted by the absorption spectrum of the phytoplankton.

For measured profiles, we averaged the standard incident spectrum, $I_0(\lambda)$, over the half-power bandwidths of the interference filters, which were adjusted so that the integral over the visible spectrum was the same as the smooth curve. We then predicted the PFD at depth z in 5-cm increments, $I_z(\lambda)$, by the empirical relation

$$I_z(\lambda) = I_0(\lambda) \exp[-k_d(\lambda)\, z]. \quad (7)$$

Furthermore, we interpolated a value for the missing $k_d(550)$, assuming an exponential decline between 500 and 600 nm with a spectral slope of 0.011 [i.e. the median of the spectral slopes of $a_d(\lambda)$ and $a_x(\lambda)$]. We then determined PUR per unit of Chl, PUR(z) from the relation

$$\mathrm{PUR}(z) = \Sigma\, I_z(\lambda)\, a^*_{ph}(\lambda). \quad (8)$$

The photic depth based on PUR, z_p(PUR), was determined as the depth at which PUR(z) was reduced to 1% of the surface value. A similar procedure was used with model estimates of $k_d(\lambda)$, except that $I_0(\lambda)$ and $a^*_{ph}(\lambda)$ were not averaged over the half-power bandwidths of the interference filters before integration over λ. Predicted z_p(PUR) was unbiased with respect to that calculated from measurements of $k_d(\lambda)$ (Fig. 9a). The rms error of predictions is 0.37 m and is fairly constant across a range of observed z_p(PUR) from 1.5 to 4.5 m.

Photosynthetically active radiation (PAR)—Photic depths based on penetration of PAR, z_p(PAR), were calculated from measurements of $k_d(\lambda)$ as above for PUR, except that calculated values of PFD were not weighted by $a^*_{ph}(\lambda)$. Photic depths calculated in this way compared favorably with those determined with a broadband 4π sensor (Fig. 9b), while z_p(PAR) was highly correlated with z_p(PUR), but biased, especially for shallow photic depths (Fig. 9c). Secchi depth, z_{SD}, was highly correlated with both z_p(PUR) and z_p(PAR); z_p(PUR) can be estimated from Secchi depth by the regression $z_p(\mathrm{PUR}) = 2.7 z_{SD} + 0.35$ (Fig. 9d).

The inverse model—In principle, the four parameters, [MSS], [TSS], [DOC], and [Chl *a*] could be estimated from measurements of $k_d(\lambda)$ by estimating b from $k_d(720)$ and rearranging Eq. 4 to determine [MSS], followed by solution of the matrix equation

$$\begin{bmatrix} a^*_d(410) & a^*_x(410) & a^*_{ph}(410) \\ \vdots & \vdots & \vdots \\ a^*_d(690) & a^*_x(690) & a^*_{ph}(690) \end{bmatrix} \times \begin{bmatrix} \mathrm{DOC} \\ \mathrm{TSS} \\ \mathrm{Chl}\ a \end{bmatrix} = \begin{bmatrix} a_t - a_w(410) \\ \vdots \\ a_t - a_w(690) \end{bmatrix} \quad (9)$$

to determine [DOC], [TSS], and [Chl *a*], where a^*_d and a^*_x are exponential terms on the right-hand sides of Eq. 5 and 6. (The nonzero intercepts in Eq. 5 and 6 are ignored for this analysis.)

[MSS] estimated by rearranging Eq. 4 fell about the 1 : 1 prediction line, but the scatter was considerable. The coefficient of determination between predicted and observed concentrations was only 0.44. Attempts to obtain a least-squares solution of Eq. 9 by the singular value decomposition method (Press et al. 1986) gave large positive and negative values for [DOC] and [MSS] due to the similarity in shapes of $a^*_d(\lambda)$ and $a^*_x(\lambda)$; we abandoned further attempts to determine [DOC] and [MSS] from optical measurements. As an alternative procedure we postulated that, in this eutrophic system, deviation of absorption at 670 nm above that due to water would be a good predictor of [Chl *a*]. A plot of [Chl *a*] against $a_t(670) - a_w(670)$ (Fig. 10a) is linear over the observed range with most points falling close to the line predicted by the relation

$$[\mathrm{Chl}\ a] = [a_t(670) - a_w(670)]/a^*_{ph}(670)$$

where the value of $a^*_{ph}(670)$ is the mean

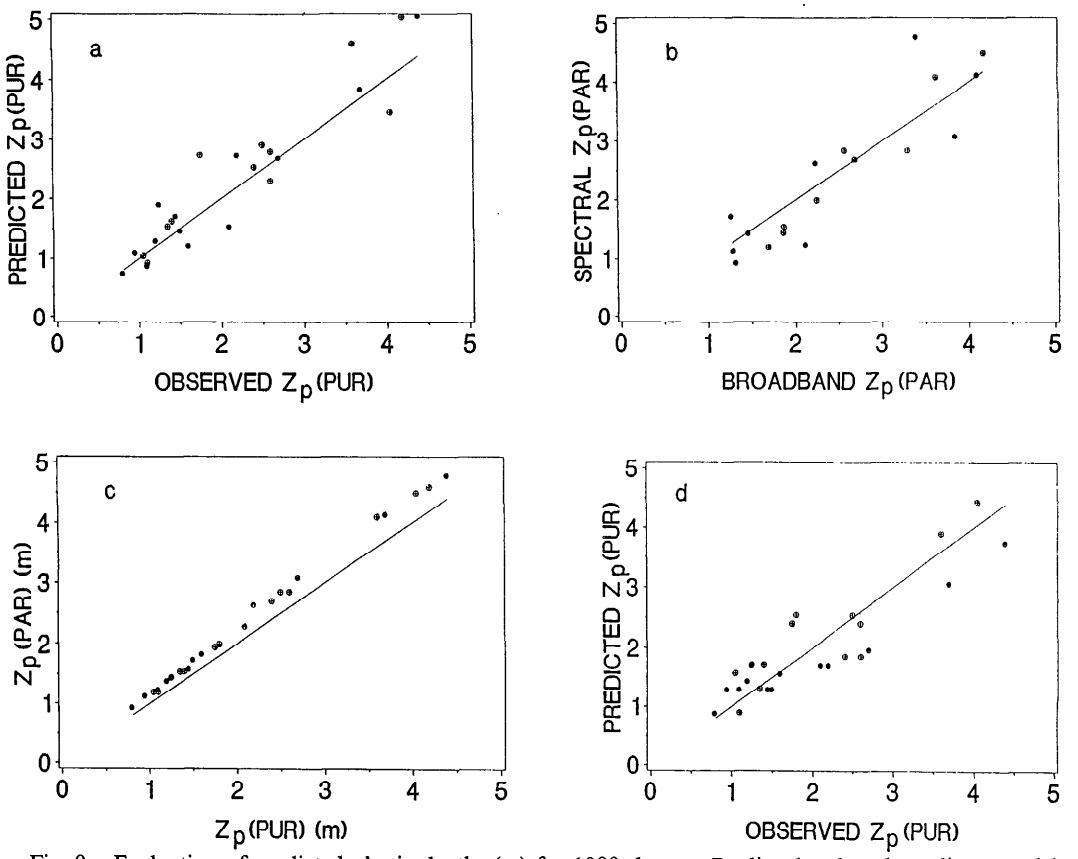

Fig. 9. Evaluation of predicted photic depths (m) for 1989 data. a. Predicted z_p based on direct model; observed z_p based on measured $k_d(\lambda)$. b. Spectral z_p based on measured $k_d(\lambda)$; broadband z_p calculated from measurements of quantum scalar irradiance (400–700 nm). c. Photic depth for both PUR and PAR calculated from measurements of $k_d(\lambda)$. d. Predicted z_p estimated from regression against Secchi depth; observed z_p calculated from measured $k_d(\lambda)$. ●—1988 data; ⊕—1989 data.

determined by laboratory measurements (Table 4). Several of the outliers of this relationship are brought closer to observed values by dividing by the measured $a^*_{ph}(670)$ rather than the mean (Fig. 10b), suggesting that biological variability in $a^*_{ph}(\lambda)$ places fundamental constraints on the precision of estimates of [Chl *a*] from measurements of diffuse attenuation.

Discussion

Optical coefficients—We estimated scattering coefficients from the model of Kirk (1984) under the assumption that water is the only absorbing substance in the 720-nm waveband. In vivo absorption spectra of phytoplankton show negligible absorbance above 710 nm (Jeffrey 1981). The strong negative exponential decay of absorbance by dissolved substances and by particles on depigmented filters suggest that absorbance by these constituents should also be negligible in the 720-nm waveband. Absorbance above 700 nm measured spectrophotometrically on filtrates is usually attributed to scattering by residual particles passing the filter (Bricaud et al. 1981). Thus, to the extent that this assumption is valid, the accuracy of estimated b at 720 nm depends systematically on the validity of Eq. 2 and systematically and randomly on the estimate of $k_d(720)$.

Equation 2 has not been verified independently, due to the difficulty of estimating scattering coefficients in situ. It is, however, based on an empirical fit to results of a Mon-

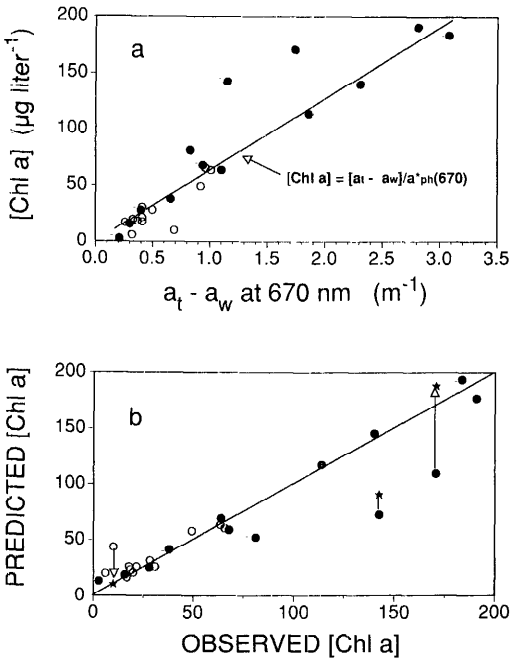

Fig. 10. a. Dependence of [Chl *a*] on water-corrected absorption at 670 nm: O—1988; ●—1989; equation of solid line is given on graph; $a^*_{ph}(670)$ estimated from laboratory measurements of particulate absorbances. b. Predicted and observed [Chl *a*]: ★—change in prediction when measured rather than mean a^*_{ph} is used to make prediction. Other symbols as in panel a.

te Carlo model that has relatively unrestrictive assumptions; the fit of Eq. 2 to the model results used to derive it is quite good (Kirk 1984), thus we expect measurement errors in $k_d(720)$ to be of greater concern. The need to apply Eq. 2 in waters where $b/a_t(\text{min})$ exceeded 20 (Table 2), however, and where there were vertical inhomogeneities (Table 5, Fig. 8), suggests that exploration of these realms with Monte Carlo methods could produce needed results (*see also* Bannister 1990).

Correspondence between z_p(PAR) estimated from spectral measurements with that estimated with the commercially available PAR sensor suggests that systematic bias in our k_d measurements should be small. Coefficients of variation for estimates of $k_d(720)$ ranged from <2% for the lowest values to 7% for the highest. At the lowest values of $k_d(720)$ (1.2 m^{-1}) a 2% deviation translates to a 10% deviation in estimated b; at the highest value (3.8 m^{-1}), a 7% deviation in estimated $k_d(720)$ translates to a 15% deviation in estimated b. The amplification of error is due to the quadratic dependence of b on $k_d(720)$. The range of b estimated here is very similar to that determined by Kirk (1981) for turbid inland waters of Australia having a similar range of photic depth.

Estimation of absorption coefficients at other wavelengths depends on the assumption of spectrally constant scattering coefficients. Phillips and Kirk (1984) verified this assumption experimentally and gave arguments for expecting such behavior. Witte et al. (1982) found minimal wavelength dependence for backscattering coefficients in systems in which scattering was dominated by inorganic solids. For some species of algae absorption and scattering are complementary, i.e. scattering is depressed in wavebands where absorption is strong (Bricaud et al. 1988), and, at the high [Chl] examined here, such an effect could introduce wavelength dependence of b. The significance of this effect for natural waters is difficult to evaluate because different species of algae displayed opposing spectral trends in scattering cross section. Thus, to a first approximation, major variations in b appear to be governed by changes in the concentrations of particles in suspension, but verification of spectral invariance of b in this system must await completion of a spectral transmissometer (under construction) having wavebands matching the radiometer.

The model developed to predict absorption coefficients from measured water quality parameters utilized in situ data only for determination of β; furthermore, the mean value, 3.31, is close to the value of 2.69 (Gallegos unpubl. data) determined on a laboratory culture of *Gyrodinium uncatenum* with the method of Kishino et al. (1985). Our ability to accurately predict diffuse attenuation coefficients for all wavelengths (Figs. 6, 7) from the sum of specific absorbances due to water-quality constituents and estimated scattering coefficients suggests that true absorption and scattering coefficients are being estimated from the in situ profiles.

Estimates of b were linearly related to [MSS] (Fig. 4a, Table 3). The estimated scattering cross section (2.41 $m^2\ g^{-1}$) is con-

siderably higher than the range (0.51–0.68 m^2 g^{-1}) estimated by Bukata et al. (1981) for western Lake Ontario. There may be qualitative differences (e.g. particle size, degree of aggregation) in the mineral particulates in the two systems. Also, Bukata et al. made their observations at much lower concentrations of suspended solids, which exceeded 3 mg liter^{-1} on only one sampling date. Their scattering cross sections predict a spectral mean scattering coefficient of 1.79 m^{-1} at 2.5 mg liter^{-1} of MSS, within our range of values (1.7–2.8 m^{-1}) estimated for the three stations having [MSS] <3 mg liter^{-1} (Table 2). That is, at [MSS] <3 mg liter^{-1}, the noise in our measurements easily admits a much lower scattering cross section, but over the total range of concentrations observed here, the higher value is required.

Direct and inverse models—From laboratory measurements we determined specific absorption curves for dissolved matter, Chl and associated pigments, and nonchlorophyllous particles. In developing the specific curves, the absorption coefficients extracted from the in situ optical profiles were used only in calculating an estimated pathlength amplification factor for proper scaling of the $a^*_{ph}(\lambda)$ and $a^*_x(\lambda)$ curves (Eq. 1b). The 400-nm intercepts of the $a_d(\lambda)$ and $a_x(\lambda)$ curves were linearly related to [DOC] and [TSS] respectively, allowing us to estimate the total absorption coefficient from measurements of [DOC], [TSS], [Chl *a*], and tabulated values of $a_w(\lambda)$. The linear relationship between estimated b and [MSS] completed the set of equations for estimating $k_d(\lambda)$ with Eq. 2.

In general, none of the specific absorption curves was constant, and $a^*_{ph}(\lambda)$ showed the most variability (Fig. 5). The regressions that scaled the specific curves by water-quality parameters exhibited varying degrees of scatter (r^2 = 0.8–0.9, Fig. 4, Table 2). Consequently, most profiles exhibited some systematic departure from model estimates in certain regions of the spectrum (Fig. 6). Over the entire data set however, model predictions of both diffuse attenuation (Fig. 7) and photic depths (Fig. 9a) were unbiased for both the development and the evaluation data sets. For many purposes, it is possible to bypass use of the specific curves and water-quality scalars. Direct measurement of $a_p(\lambda)$ and $a_d(\lambda)$ in the laboratory is generally easier than measurement of the parameters ([Chl], [TSS], and [DOC]) required to scale the specific curves. When available, actual measurements of $a_p(\lambda)$ and $a_d(\lambda)$ can be used to predict $a_t(\lambda)$, thereby avoiding the sometimes large uncertainty incurred by using a mean Chl-specific absorbance curve; to predict $k_d(\lambda)$ in these waters, it is still necessary to estimate b with measurements of [MSS] and Eq. 4.

How site-specific is the direct model? At the most fundamental level, the general approach used to develop the model can only be used in waters for which Eq. 2 is applicable. The limiting factor is that the volume-scattering phase function used by Kirk (1981, 1984) is specific to "turbid" waters. In general the shape of the scattering phase function remains constant for total scattering coefficients >0.2 m^{-1} (Phillips and Koerber *cited by* Phillips and Kirk 1984), and Phillips and Kirk (1984) sucessfully used the approach in waters considerably more oligotrophic than those examined here. Qualitatively, the model will predict "blue water" characteristics at low concentrations of all constituents; but the y-intercepts of all regressions are quite uncertain (Table 3, Fig. 4). Therefore quantitative extrapolation to waters clearer than those used for model development is unadvisable. It is interesting to note, however, that extrapolation to conditions more turbid than those encountered in the development data set was successful (Fig. 9, ●).

Two additional qualifications should also be noted. Equation 4 predicts b solely on the basis of [MSS]. Prieur and Sathyendranath (1981) found b to be related to [Chl *a*], but the relationship varied regionally, and there was no relationship for stations with U-shaped absorption spectra (i.e. those resembling Fig. 6b). Weidemann and Bannister (1986) also found a more or less linear relationship between b and Chl in Irondequoit Bay, with the scatter bracketed by lines having Chl-specific scattering cross sections from 0.06 to 0.12 m^2 (mg Chl *a*)$^{-1}$. They also used Kirk's (1984) method for extracting b from optical profiles. Interestingly,

Weidemann and Bannister found no relationship between b and Chl when the system was dominated by *Peridinium* and centric diatoms. Dinoflagellates were dominant in most of our summer profiles. Furthermore, only three of our estimates of b fell within the range observed by either Prieur and Sathyendranath (1981) or Weidemann and Bannister (1986) (i.e. <5 m^{-1}). Thus MSS appeared to dominate all other sources of scattering in our data, but this will not be true everywhere, even in coastal waters.

Secondly, methods for chemical determination of [DOC] are currently being reevaluated (Sugimura and Suzuki 1988; Jackson 1988; Williams and Druffel 1988). If we are systematically underestimating [DOC] then the slope of the regression in Eq. 5 would need to be reduced. It is not possible to predict what would happen to the precision of the relationship if alternate chemical methods were used.

These considerations suggest that the model should be applied only to turbid estuaries and coastal waters with [MSS] >1 mg liter^{-1} and [DOC] (as conventionally measured) $\gtrsim 2$ mg liter^{-1}. In terms of optical coefficients, the restrictions are $b \geq 1$–2 m^{-1}, and $a_d(400) \geq 1$ m^{-1}. With these restrictions met, site specificity should depend on the degree to which the shapes of the specific curves and the regressions to scale them vary regionally. Our curve of $a^*_d(\lambda)$ is similar to that determined by Bricaud et al. (1981) for a wide distribution of oceanic regions, and the spectral slope we determined (0.012 nm^{-1}) is within but near the low end of the range (0.011–0.018 nm^{-1}) summarized by Roesler et al. (1989). Regressions to scale the relationship between absorbance and [DOC] can be site specific, however, over rather short distances (Wheeler 1977). The characteristic shape of the absorption spectrum due to particulate detritus has not been widely studied; Maske and Haardt (1987) indicated that the shapes of $a_d(\lambda)$ and $a_x(\lambda)$ were very different from one another in Kiel Harbor, whereas Roesler et al. (1989) found very similar spectral shapes for particulate detritus and DOM. Our spectral slope for particulate detritus, 0.0104 nm^{-1}, is near the mean of published values, 0.011 nm^{-1}, as summarized by Roesler et al. (1989). A more detailed comparison of the Rhode River with similar measurements in the Indian River estuary of eastern Florida will be presented elsewhere.

Complete solution of the inverse problem was not possible. It was possible, however, to estimate [MSS] and [Chl a] from the optical profiles because of the unique relationship that these parameters had with optical properties at 720 and 670 nm, respectively. The relationship between b and [MSS] exhibited greater scatter in the 1989 data than in the data from 1988. Estimation of [MSS] from estimated b is more sensitive to this scatter than is the direct problem (i.e. estimation of k_d) due to the linear dependence of [MSS] on b (Eq. 4), as opposed to the square-root dependence of k_d on b (Eq. 2). Consequently the C.V. between predicted and observed [MSS] was only 0.44. Estimated [Chl a] showed better correspondence with measured values, despite the necessity to extrapolate the estimation relationship to concentrations exceeding, by a factor of 2, those encountered in its development. The fact that estimates for several profiles could be improved by using measured $a^*_{ph}(670)$ rather than the mean gives further evidence that actual absorption coefficients are being observed.

The present modeling effort has demonstrated the utility of Eq. 2 in waters considerably more turbid than those in which it was previously applied (Phillips and Kirk 1984; Weidemann and Bannister 1986). The use of characteristic curves to reconstruct the in situ absorption spectrum is on sounder theoretical footing than regressions between diffuse attenuation coefficients and water-quality parameters. Although it is still necessary to scale the specific curves according to statistical regressions, the slopes of the regressions represent absorption and scattering cross sections of the measured constituents, and hence have physical meaning. There remains hope that further study of the variability of these coefficients in terms of measurable qualities of the various dissolved and particulate materials will lead to further improvement of the model.

References

BANNISTER, T. T. 1990. Empirical equations relating scalar irradiance to *a*, *b/a*, and solar zenith angle. Limnol. Oceanogr. **35:** 173–177.

BRICAUD, A., A.-L. BÉDHOMME, AND A. MOREL. 1988. Optical properties of diverse phytoplanktonic species: Experimental results and theoretical interpretation. J. Plankton Res. **10:** 851–873.

———, A. MOREL, AND L. PRIEUR. 1981. Absorption by dissolved organic matter of the sea (yellow substance) in the UV and visible domains. Limnol. Oceanogr. **26:** 43–53.

BUKATA, R. P., J. H. JEROME, J. E. BRUTON, S. C. JAIN, AND H. H. ZWICK. 1981. Optical water quality model of Lake Ontario. 1: Determination of the optical cross sections of organic and inorganic particulates in Lake Ontario. Appl. Opt. **20:** 1696–1703.

GOLDBERG, B., W. H. KLEIN, D. L. CORRELL, AND J. W. PIERCE. 1985. Instrumentation for performing spectral measurements in a marine environment. J. Mar. Technol. Soc. **18:** 4, 6.

HANDBOOK OF CHEMISTRY AND PHYSICS. 1980. 58th ed. Chem. Rubber Co.

JACKSON, G. A. 1988. Implications of high dissolved organic matter concentrations for oceanic properties and processes. Oceanography **1:** 28–33.

JEFFREY, S. W. 1981. Algal pigment systems, p. 33–58. *In* Primary productivity in the sea. Brookhaven Symp. Biol. 31. Plenum.

———, AND G. F. HUMPHREY. 1975. New spectrophotometric equation for determining chlorophyll *a*, *b*, c^1, and c^2 in higher plants, algae, and natural phytoplankton. Biochem. Physiol. Pflanz. **167:** 191–194.

JERLOV, N. 1976. Marine optics. Elsevier.

KIEFER, D. W., AND J. B. SOOHOO. 1982. Spectral absorption by marine particles of coastal waters of Baja California. Limnol. Oceanogr. **27:** 492–499.

KIRK, J. T. O. 1981. Monte Carlo study of the nature of the underwater light field in, and the relationships between optical properties of, turbid yellow waters. Aust. J. Mar. Freshwater Res. **32:** 517–532.

———. 1983. Light and photosynthesis aquatic ecosystems. Cambridge.

———. 1984. Dependence of relationship between apparent and inherent optical properties of water on solar altitude. Limnol. Oceanogr. **29:** 350–356.

KISHINO, M., N. OKAMI, M. TAKAHASHI, AND S. ICHIMURA. 1986. Light utilization efficiency and quantum yield of phytoplankton in a thermally stratified sea. Limnol. Oceanogr. **31:** 557–566.

———, M. TAKAHASHI, N. OKAMI, AND S. ICHIMURA. 1985. Estimation of the spectral absorption coefficients of phytoplankton in the sea. Bull. Mar. Sci. **37:** 634–642.

MASKE, H., AND H. HAARDT. 1987. Quantitative in vivo absorption spectra of phytoplankton: Detrital absorption and comparison with fluorescence excitation spectra. Limnol. Oceanogr. **32:** 620–633.

MITCHELL, B. G., AND D. A. KIEFER. 1984. Determination of absorption and fluorescence excitation spectra for phytoplankton, p. 157–169. *In* O. Holm-Hansen et al. [eds.], Marine phytoplankton and productivity. Springer.

MOREL, A. 1981. Available, usable, and stored radiant energy in relation to marine photosynthesis. Deep-sea Res. **25:** 673–688.

———. 1988. Optical modeling of the upper ocean in relation to its biogenous matter content (case I waters). J. Geophys. Res. **93:** 10,749–10,768.

PHILLIPS, D. M., AND J. T. O. KIRK. 1984. Study of the spectral variation of absorption and scattering in some Australian coastal waters. Aust. J. Mar. Freshwater Res. **35:** 635–644.

PIERCE, J. W., D. L. CORRELL, M. A. FAUST, B. GOLDBERG, AND W. H. KLEIN. 1986. Response of underwater light transmittance in the Rhode River estuary to changes in water-quality parameters. Estuaries **9:** 169–178.

PLATT, T., M. LEWIS, AND R. GEIDER. 1984. Thermodynamics of the pelagic ecosystem: Elementary closure conditions for biological production in the open ocean, p. 49–84. *In* Flows of energy and materials in marine ecosystems. NATO Conf. Ser. 4, Mar. Sci. V. 13. Plenum.

———, AND S. SATHYENDRANATH. 1988. Oceanic primary production: Estimation by remote sensing at local and regional scales. Science **241:** 1613–1620.

PREISENDORFER, R. 1976. Hydrologic optics. V. 1. NOAA.

PRESS, W. H., B. P. FLANNERY, S. A. TEUKOLSKY, AND W. T. VETTERLING. 1986. Numerical recipes, the art of scientific computing. Cambridge.

PRIEUR, L., AND S. SATHYENDRANATH. 1981. An optical classification of coastal and oceanic waters based on the specific spectral absorption curves of phytoplankton pigments, dissolved organic matter, and other particulate materials. Limnol. Oceanogr. **26:** 671–689.

ROESLER, C. S., M. J. PERRY, AND K. L. CARDER. 1989. Modeling in situ phytoplankton absorption from total absorption spectra in productive inland marine waters. Limnol. Oceanogr. **34:** 1510–1523.

SMITH, R. C., AND K. S. BAKER. 1981. Optical properties of the clearest natural waters. Appl. Opt. **20:** 177–184.

SPINRAD, R. [ED.]. 1989. Hydrologic optics. Limnol. Oceanogr. **34:** 1389–1766.

SUGIMURA, Y., AND Y. SUZUKI. 1988. A high-temperature catalytic oxidation method for the determination of non-volatile dissolved organic carbon in seawater by direct injection of a liquid sample. Mar. Chem. **24:** 105–131.

TIMOFEEVA, V. A. 1974. Optics of turbid waters (results of laboratory studies), p. 177–219. *In* N. G. Jerlov and E. Steemann Nielsen [eds.], Optical aspects of oceanography. Academic.

VAN DE HULST, H. C. 1957. Light scattering by small particles. Wiley.

WEIDEMANN, A. D., AND T. T. BANNISTER. 1986. Absorption and scattering coefficients in Irondequoit Bay. Limnol. Oceanogr. **31:** 567–583.

WHEELER, J. R. 1977. Dissolved organic carbon:

Spectral relationships in coastal waters. Limnol. Oceanogr. **22:** 573–575.

WILLIAMS, P. M., AND E. R. M. DRUFFEL. 1988. Dissolved organic matter in the ocean: Comments on a controversy. Oceanography **1:** 14–17.

WITTE, W. G., AND OTHERS. 1982. Influence of dissolved organic materials on turbid water optical properties and remote-sensing reflectance. J. Geophys. Res. **87:** 441–446.

Submitted: 23 January 1990
Accepted: 23 April 1990
Revised: 13 July 1990